University of Bristol - Explore Bristol Research
General rights

Nonequilibrium Spatiotemporal Sensing within Acoustically Patterned Two-Dimensional Protocell Arrays

Liangfei Tian,[†] Mei Li,[†] Juntai Liu,[‡] Avinash J. Patil,[†] Bruce W. Drinkwater,[§] and Stephen Mann[*,†]

[†]Centre for Protolife Research and Centre for Organized Matter Chemistry, School of Chemistry, University of Bristol, Bristol BS8 1TS, U.K.

[‡]School of Biochemistry, Medical Sciences Building, University of Bristol, Bristol BS8 1TD, U.K.

[§]Faculty of Engineering, Queens Building, University of Bristol, Bristol BS8 1TR, U.K.

S Supporting Information

ABSTRACT: Acoustically trapped periodic arrays of horse-radish peroxidase (HRP)-loaded poly-(diallydimethylammonium chloride) / adenosine 5′-triphosphate coacervate microdroplet-based protocells exhibit a spatiotemporal biochemical response when exposed to a codiffusing mixture of substrate molecules (o-phenylenediamine (o-PD) and hydrogen peroxide (H_2O_2)) under nonequilibrium conditions. Unidirectional propagation of the chemical concentration gradients gives rise to time- and position-dependent fluorescence signal outputs from individual coacervate microdroplets, indicating that the organized protocell assembly can dynamically sense encoded information in the advancing reaction-diffusion front. The methodology is extended to arrays comprising spatially separated binary populations of HRP- or glucose oxidase-containing coacervate microdroplets to internally generate a H_2O_2 signal that chemically connects the two protocell communities via a concerted biochemical cascade reaction. Our results provide a step toward establishing a systematic approach to study dynamic interactions between organized protocell consortia and propagating reaction-diffusion gradients, and offer a new methodology for exploring the complexity of protocellular communication networks operating under nonequilibrium conditions.
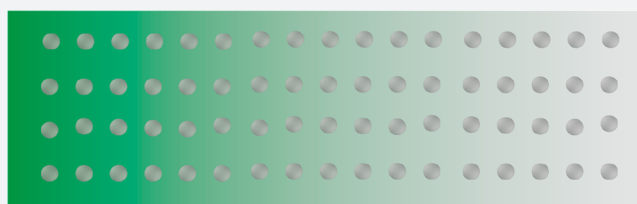
INTRODUCTION

The remarkable adaptivity of individual cells and cell communities relies fundamentally on their ability to dynamically sense and respond to spatial and temporal changes in molecular concentration fields present in the local environment.[1,2] Processes such as cell differentiation and spatial organization,[3] chemotaxis,[4] cell division,[5] and site-specific DNA targeting by proteins[5] are regulated in part by signaling cues associated with chemical diffusion gradients produced under nonequilibrium conditions. A range of innovative biomimetic approaches have been developed to study these complicated reaction-diffusion systems.[6−9] Mimicking such adaptivity in rudimentary artificial cell-like constructs (protocells)[10−14] could lead to a better understanding of the emergence of biological complexity and also provide an initial step toward developing future microscale technologies exhibiting key features of living systems.[15−18] Recent developments have shown that different types of model protocells exhibit a certain level of capability to dynamically respond to their environment,[19−23] each other,[24−27] or biological cells,[28,29] and in so doing convert external stimuli to specific protocellular responses.

Coacervate microdroplets produced by electrostatic complexation between oppositely charged macromolecular or molecular components have been exploited as molecularly crowded membrane-free synthetic protocells[30−34] capable of enhanced enzymatic activity,[35] in vitro gene expression,[36] and nonequilibrium electric field-induced energization.[37] Recently, coacervate microdroplets prepared from charge-balanced mixtures of poly(diallydimethylammonium chloride) (PDDA) and adenosine 5′-triphosphate (ATP) were spontaneous assembled and spatially trapped into periodic arrays using an acoustic (ultrasonic) standing wave pressure field.[38] Primary microdroplets of the PDDA/ATP coacervate phase along with sequestered molecules and nanoparticles were trapped at the pressure nodes and slowly sedimented under gravity onto the glass substrate where they locally coalesced to produce a defect-free square array of single droplets typically 50−100 μm in diameter and spaced at a uniform distance of 110 μm. Compared with a dispersion of randomly mixed droplets, each synthetic protocell in the patterned community can be indexed with respect to their spatial positions and attendant chemical activity over a wide range of time scales. As a consequence, it should be possible to expose the arrays to unidirectional reaction-diffusion gradients under nonequilibrium conditions to establish a transient spatiotemporal response across the organized protocell community to produce signal outputs for example for enzymatically catalyzed biochemical reactions.[39]
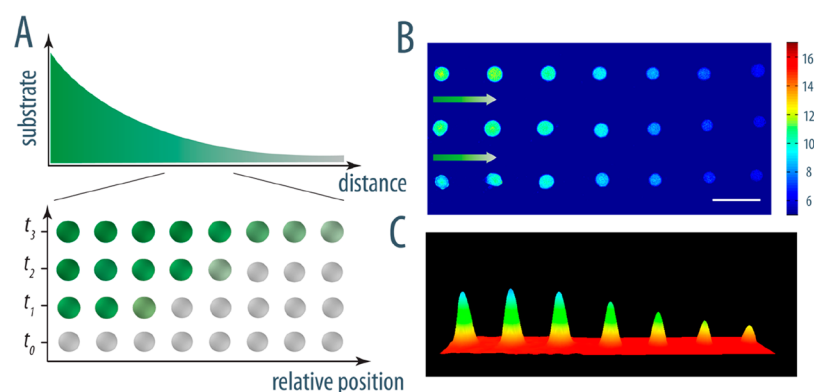
Figure 1. Nonequilibrium biochemical sensing in 2D protocell arrays. (A) Schematic representation of a 1D substrate concentration gradient established by unidirectional diffusion into a 2D array of enzymatically active PDDA/ATP coacervate microdroplets (top), and spatiotemporal response of droplets (bottom); the reaction-diffusion gradient is established along the x direction (distance, relative position) of the 2D microdroplet array. (B) Fluorescence microscopy image recorded 5.5 min after onset of unidirectional codiffusion (arrows) of H_2O_2/o-PD (20 μL, 50/25 mM) into a square array of acoustically trapped HRP-containing PDDA/ATP coacervate microdroplets showing a gradient in 2,3-DAP fluorescence intensity along the x axis. The onset of 2,3-DAP production is associated with propagation of the substrate diffusion front. The image is recorded from the central region of the acoustically patterned array (see Figure S1); scale bar, 100 μm. (C) Corresponding 3D surface plot of 2,3-DAP fluorescence intensity for the middle row of the HRP-containing droplets shown in (B).

We demonstrate this principle by preparing acoustically trapped, two-dimensional (2D) square grids of horseradish peroxidase (HRP)-loaded PDDA/ATP microdroplets, and exposing the arrays to an advancing codiffusing flux of enzyme substrates (o-phenylenediamine (o-PD) and hydrogen peroxide (H_2O_2)) to produce concentration gradients and chemical diffusion fronts that propagate unidirectionally across the microdroplet assembly (Figure 1A). We follow the spatial and temporal signal outputs of individual protocells in the array by measuring the green fluorescence associated with the production and sequestration of 2,3-diaminophenazine (2,3-DAP; coacervate partition constant = 37) by HRP/H_2O_2-mediated oxidation of o-PD in each droplet.[40] Our results indicate that the 2D array can dynamically sense the encoded information in the advancing concentration gradients to generate a spatiotemporal biochemical response under nonequilibrium conditions. Finally, we extend our methodology to elicit a spatiotemporal biochemical response via internally derived molecule-based signaling within the droplet array. For this, we prepare patterned PDDA/ATP droplet 2D arrays comprising two spatially separated protocell populations containing either HRP or glucose oxidase (GOx) and expose the system to a unidirectional flux of glucose and o-PD. A cascade reaction is established between the two protocell communities via the in situ generation and propagation of a H_2O_2 reaction-diffusion front, which in turn produces a time- and space-dependent response in the production of 2,3-DAP specifically in the HRP-functionalized population.

Taken together, our results provide a step toward establishing a systematic approach to studying dynamic interactions between organized protocell communities and propagating reaction-diffusion gradients, and offer a new methodology for exploring the complexity of protocellular communication networks operating under nonequilibrium conditions.

■ **RESULTS**

A square, grid-like array of HRP-containing PDDA/ATP coacervate microdroplets was prepared by injecting a premixed solution of PDDA and HRP into the chamber of a custom-built acoustic trapping device containing an aqueous ATP

solution and operating under a periodic 2D standing pressure field generated at 6.76/6.78 MHz (see Methods and Figure S1). Three-dimensional (3D) confocal fluorescence microscopy images of the acoustically trapped coacervate phase labeled with rhodamine isothiocyanate (RITC)-tagged HRP indicated that the coacervate microdroplets were assembled in situ at the nodal regions of the acoustic pressure field and strongly bound to the underlying PEGylated glass substrate in the presence or absence of the acoustic field, and that HRP was strongly sequestered within the protocells (Figure S2). Profiles across individual rows of the microdroplets showed similar mean fluorescence intensities, indicating that the droplets had comparable enzyme concentrations (Figure S3).

To induce dynamical responses in the periodically ordered HRP-active droplets under nonequilibrium conditions, we switched off the acoustic pressure field and injected an aqueous solution containing H_2O_2 and o-PD (H_2O_2/o-PD; 20 μL, 50/25 mM) into the device specifically from one edge of the chamber to produce an advancing reaction-diffusion gradient in both substrates across the microdroplet array. Fluorescence microscopy images recorded in the viewing window indicated a spatiotemporal peroxidase response to the codiffusion of substrates across the droplet array (Figure 1B). In general, the green fluorescence intensity associated with formation and sequestration of the reaction product (2,3-DAP) within the individual microdroplets progressively decreased along individual rows of droplets lying parallel to the direction of diffusion (x axis) (Figure 1C). In contrast, droplets aligned perpendicular to the diffusion front (y axis) showed minimal differences in fluorescence intensity along the individual rows (Figure S4).

Co-diffusion of H_2O_2 and o-PD (H_2O_2/o-PD; 20 μL, 50/25 mM) into a 2D periodic array of HRP-containing PDDA/ATP coacervate microdroplets was monitored by analysis of time-dependent fluorescence microscopy images (Figure 2A−D). The corresponding average intensity profiles (Figure 2E) recorded across a single row of protocells aligned along the direction of diffusion (x axis) revealed that the HRP activity was switched on sequentially according to the proximity of the microdroplets to the diffusion front. The relative spatiotemporal responses of each microdroplet in the array were
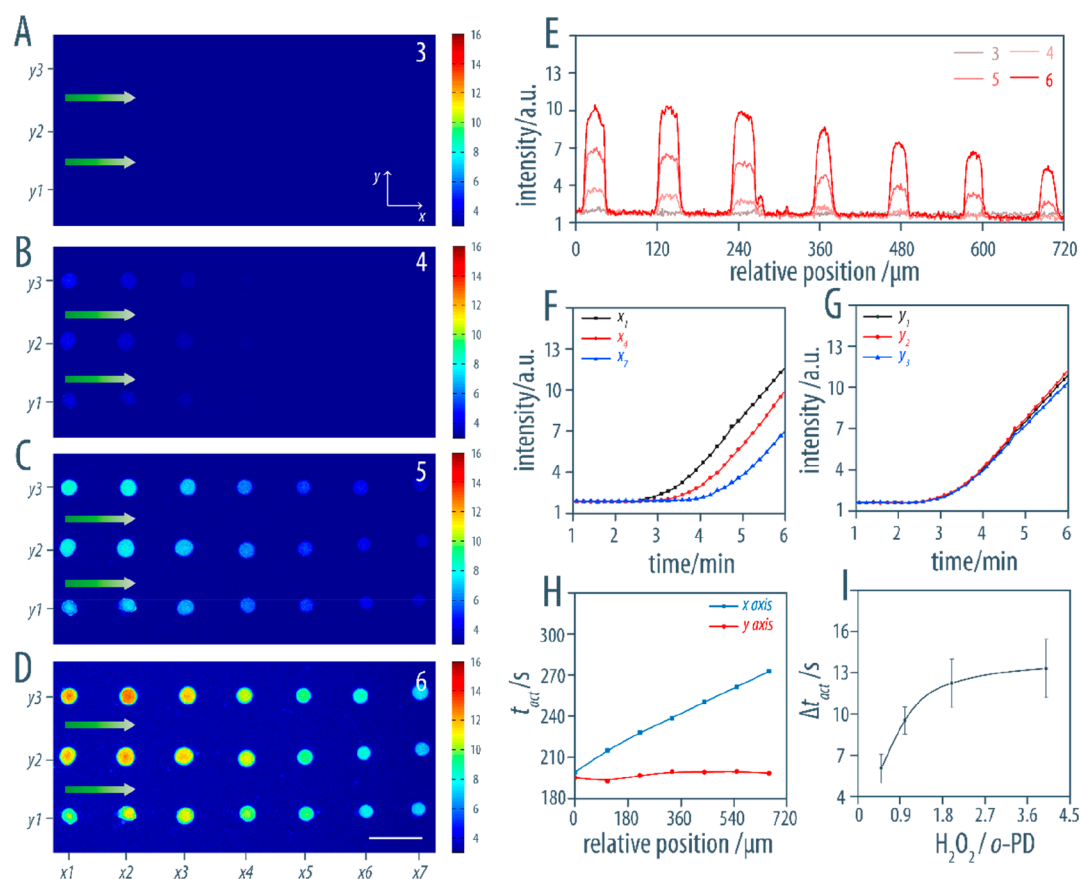
Figure 2. Spatiotemporal responses in periodic 2D arrays of enzyme-containing coacervate protocells. (A−D) Time-dependent fluorescence microscopy images recorded at 3, 4, 5, and 6 min after onset of unidirectional codiffusion of H_2O_2 and o-PD (arrows) (H_2O_2/o-PD; 20 μL, 50/25 mM) parallel to the x axis of a 2D array of HRP-containing PDDA/ATP coacervate microdroplets. Droplet positions are labeled as (x_n, y_m); scale bar, 100 μm. (E) Corresponding plots of the average fluorescence line intensity profiles recorded along the x axis for seven droplets (x_n, $n = 1−7$) located in row y_2 as shown in A−D. Profiles were recorded 3, 4, 5, and 6 min after onset of H_2O_2/o-PD codiffusion. (F) Plots of time-dependent changes in 2,3-DAP fluorescence mean intensity (a.u., arbitrary units) for three different microdroplets positioned along the x axis in row y_2 of the array shown in A−D. The three droplets are located in positions x_1 (black), x_4 (red), and x_7 (blue). Propagation of the diffusion front along the x axis results in a series of increasing activation times for the onset of 2,3-DAP production. (G) As for (F), but for three droplets (y_1 (black), y_2 (red), and y_3 (blue), positioned in row x_1 lying perpendicular to the diffusion direction showing simultaneous 2,3-DAP production. (H) Plots showing the distance-dependent (relative position) time periods required for the onset of enzyme-mediated activation (t_{act}) along a single row of seven HRP-containing coacervate microdroplets aligned parallel (blue, x axis; x_n, $n = 1−7$) or perpendicular (red, y axis; y_m, $m = 1−7$) to the H_2O_2/o-PD codiffusion front. A constant lag time (Δt_{act}) of ca. 12 s is observed for adjacent droplets aligned along the x axis and exposed to a codiffusing substrate mixture prepared with a H_2O_2: o-PD molar ratio of 2:1 (final concentrations; 1 and 0.5 mM, respectively). (I) Plot of the average lag time (Δt_{act}) measured between adjacent droplets in a single row aligned parallel to a codiffusing substrate mixture prepared at different H_2O_2: o-PD molar ratios at a constant o-PD final concentration of 0.5 mM. The average lag times decrease as the substrate molar ratios are reduced below 2.0 due to the effect of increasing relative amounts of o-PD on the enzyme-reaction kinetics.

investigated by plotting changes in the mean fluorescence intensity associated with 2,3-DAP production and sequestration as a function of time and position along the x or y axis (Figure 2F,G). All the plots revealed an induction time of ca. 3 min that was associated with the time required for the substrate molecules to codiffuse into the central viewing window after injection at one side of the device. Moreover, the relative initial rate of change in mean 2,3-DAP fluorescence intensity was constant ($6.278 \times 10^{-2} \pm 4.49 \times 10^{-3}$ arbitrary units/s) for each droplet after substrate-induced activation, suggesting that the peroxidase reaction in each of the protocells followed a similar diffusion-controlled kinetic pathway. In general, the fluorescence associated with each microdroplet increased to a steady state value over a period of ca. 15 min, after which there was a slow decrease in intensity at each lattice point in the array due to the cessation of substrate

turnover and slow release of the sequestered 2,3-DAP into the external environment (Figure S5) .

The activation time (t_{act}) for each microdroplet in the 2D array was then determined by linearly fitting the initial rate of change in fluorescence and measuring t_{act} as the intercept with the baseline. Plots of t_{act} along a line of periodically spaced microdroplets lying parallel to the direction of codiffusion (H_2O_2: o-PD molar ratio = 2:1) revealed a distinct lag time (Δt_{act}) of ca. 12 s between adjacent protocells (Figure 2H). In contrast, values for t_{act} remained unchanged along a row of microdroplets lying perpendicular to the direction of diffusion ($\Delta t_{act} = 0$) indicating no spatiotemporal response along the y axis. Increasing the H_2O_2: o-PD molar ratio above 2.0 had minimal effect on Δt_{act} measured along the x axis, while increasing the relative amounts of o-PD in the codiffusion front (molar ratios <2) decreased the average lag times from 12 to 6 s (Figure 2I).
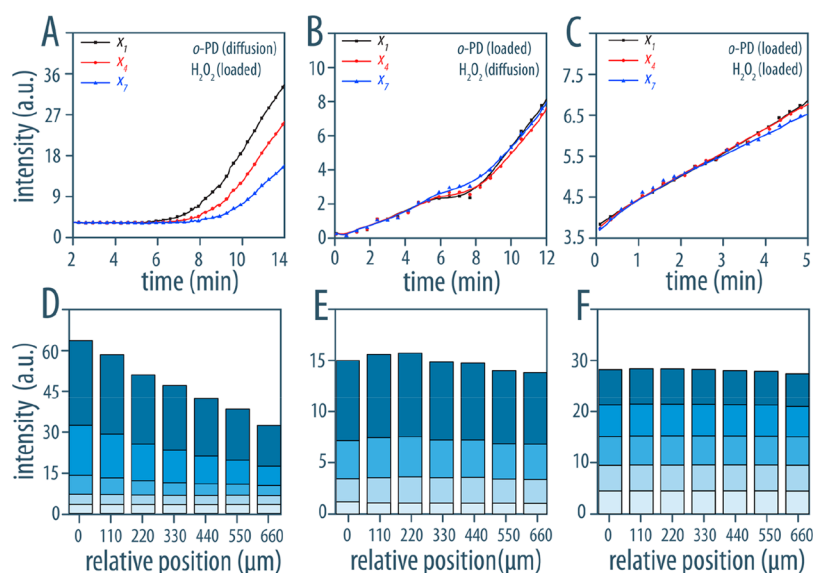
Figure 3. Influence of substrate diffusion fronts on biochemical sensing. (A, B) Plots of time-dependent changes in 2,3-DAP fluorescence mean intensity (a.u., arbitrary units) for three different HRP-containing PDDA/ATP coacervate microdroplets periodically interspaced in a row of seven protocells aligned parallel to the direction of substrate diffusion under different experimental conditions: o-PD diffusion into a 2D droplet array preloaded with H_2O_2 (A); H_2O_2 diffusion into a droplet array preloaded with o-PD (B). The three droplets are the first (x_1, black line), fourth (x_4, red line), and seventh (x_7, blue line) protocells in the row with x_1 being the first to interact with the substrate diffusion front. The variation in activation time observed for A and B is due to experimental changes in the relative distances between the injection points and edge of the chamber. The intermediate delay shown in (B) between 6 and 8 min was reproducible over several experiments. One possibility is that this period represents an initial decrease in the concentration of o-PD at the diffusion front to a level insufficient for enzyme turnover. The peroxidase reaction restarts once the local concentration of o-PD is restored by further diffusion of o-PD into the array already loaded with H_2O_2. (C) As for A and B but in the absence of a diffusion gradient (homogeneous mixing of H_2O_2/o-PD in the sample chamber containing the droplet array). (D–F) Corresponding stack bar plots determined respectively for experiments described in A–C showing the production of 2,3-DAP in a row of seven consecutive protocells aligned along the x axis. The different shades of blue bars represent the increase in fluorescence intensity over the same time interval with the lightest and darkest shades representing the first and last time periods, respectively. Time durations; 2, 3, and 1 min for D–F, respectively. Starting periods (lightest shade bar); 6–8, 0–3, and 0–1 min for D–F, respectively.
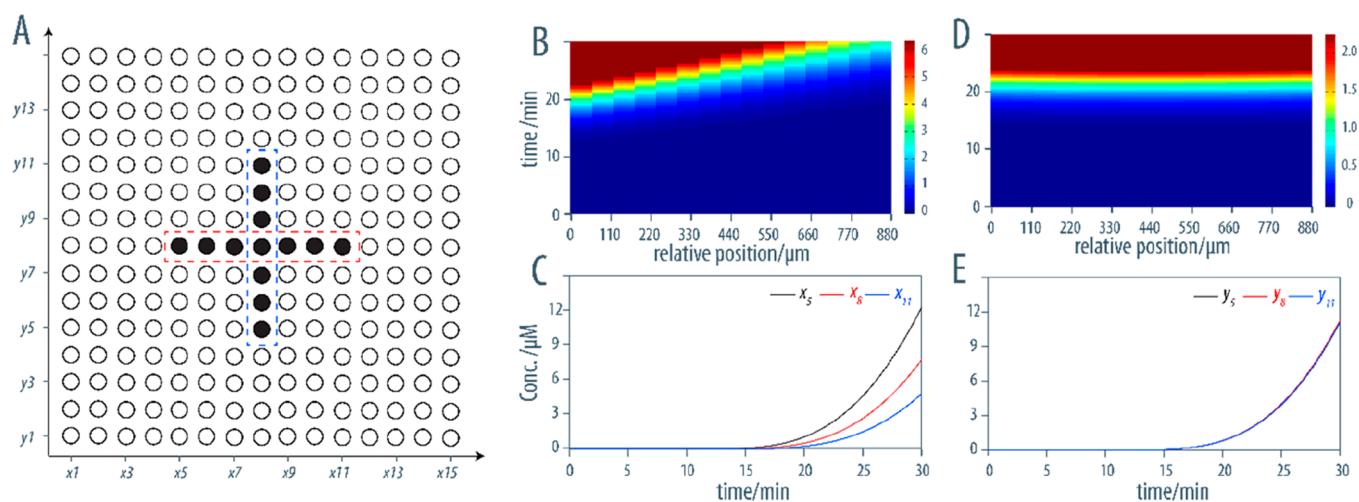

Figure 4. Simulated spatial/temporal distributions of H_2O_2 concentrations in the acoustic trapping chamber. (A) Schematic representation of the simulated area consisting of a 15 × 15 droplet array. The substrate concentration gradient and diffusion direction are aligned along the x axis. Diameter of droplets (white circles) at each lattice point = 55 μm; lattice center-to-center spacing = 110 μm. Filled circles delineated by dashed rectangles refer to simulations shown in B–E. (B) Simulated 2D plot of the spatial and temporal distributions of H_2O_2 concentration in a row of protocells aligned parallel to the H_2O_2 diffusion direction (y_8; red dashed rectangle in A). (C) Corresponding time-dependent changes in H_2O_2 concentration at three different positions (x_5, x_8, and x_{11}) along row y_8. (D) Simulated 2D plot of the spatial and temporal distributions of H_2O_2 concentration in a line of protocells aligned perpendicular to the diffusion of H_2O_2 (x_8; blue dashed rectangle in A). (E) Corresponding time-dependent changes in H_2O_2 concentration at three different positions (y_5, y_8, and y_{11}) along column x_8. Simulations are for an injection of 10 μL of H_2O_2 (50 mM) solution along the x axis. The unit for the color bar in B and D is μM. The simulations did not consider HRP-mediated substrate consumption during the diffusion process.
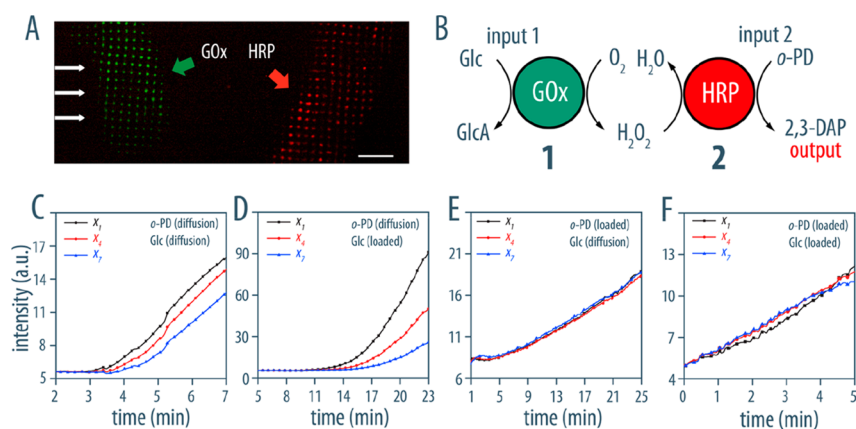
Figure 5. Substrate gradient signaling between protocell populations. (A) Representative fluorescence microscopy image showing two spatially positioned domains of acoustically patterned enzyme-containing PDDA/ATP droplet 2D arrays with sequestered FITC-tagged GOx (green; population **1**) or RITC-HRP (red; population **2**) (green and red arrows, respectively). The white arrows on the left side of the image indicate the direction of substrate diffusion; scale bar 500 μm. (B) Scheme showing bienzyme-mediated tandem reaction between two spatially separated populations of protocells. GOx-mediated oxidation of glucose (Glc) to gluconic acid (GlcA) and H_2O_2 in population **1** initiates diffusive transfer of H_2O_2 to population **2** and subsequent HRP-mediated oxidation of o-PD to fluorescent 2,3-DAP. Glucose and o-PD can be considered as inputs into populations **1** and **2**, respectively, and H_2O_2 as a signaling molecule between the two protocell communities. (C−F) Plots of representative time-dependent changes in 2,3-DAP mean fluorescence intensity (a.u., arbitrary units) for three different HRP-containing PDDA/ATP droplets (population **2**) periodically interspaced in a row of seven protocells in the red domain shown in (A) and aligned parallel to the direction of substrate diffusion under different experimental conditions: codiffusion of glucose and o-PD initially into the GOx-containing droplets (population **1**) (C); unidirectional diffusion of o-PD initially into the GOx-containing community with populations **1** and **2** preloaded with H_2O_2 (D); unidirectional diffusion of glucose into population **1** with populations **1** and **2** preloaded with o-PD (E); in the absence of a reaction-diffusion gradient (homogeneous mixing of glucose/o-PD in the sample chamber containing the two spatially separated protocell populations (F). The variations in activation time observed for C−E are due to experimental changes in the relative distances between the injection points and edge of the chamber, and between the two populations. The three droplets are the first (x_1, black line), fourth (x_4, red line), and seventh (x_7, blue line) along the same row.

Changes in the nature of the advancing reaction-diffusion front were used to determine the kinetic factors responsible for the activation and lag times recorded for microdroplets periodically ordered within the central viewing area of the acoustic trapping device. Single-component unidirectional diffusion of o-PD into a 2D droplet array preloaded with a homogeneous concentration of H_2O_2 resulted in minimal changes in induction time (typically 6 min), nonlinear production of 2,3-DAP, and a well-defined spatiotemporal response (Figure 3A). Moreover, the initial rate of 2,3-DAP production diminished along the o-PD concentration gradient (Figure 3A and Figure S6), suggesting that the substrate was progressively depleted as the reaction-diffusion front advanced through the array. Given that codiffusion of H_2O_2/o-PD produced a constant reaction rate parallel to the diffusion direction (Figure 2F and Figure S6), we attributed the decrease in initial reaction rate to the large excess of H_2O_2 preloaded into the acoustic trapping chamber. In contrast, a very short induction period (ca. 0.5 min) along with a nonpatterned response was observed when H_2O_2 was unidirectionally diffused into a droplet array preloaded with a homogeneous concentration of o-PD (Figure 3B) or in the absence of a H_2O_2 and o-PD diffusion gradient (Figure 3C). The different spatial and kinetic responses were therefore attributed to the increased rate of diffusion into the array of H_2O_2 compared with o-PD, such that the advancing o-PD diffusion front was effectively rate-determining and therefore a key factor determining the lag time (Δt_{act}) in the spatiotemporal response. Corresponding stack bar plots of the mean fluorescence intensity in a row of seven consecutive protocells aligned parallel to the diffusion direction recorded over a constant time period revealed a nonlinear increase of the

production of 2,3-DAP over time (Figure 3D−E), while a linear increase of the mean fluorescence intensity was observed in a homogeneous medium (Figure 3F), confirming that a marked concentration gradient in the o-PD diffusion front influenced the values of Δt_{act}.

The above results were consistent with 2D simulations (Figure 4A, and Figure S7 and S8) of the spatial and temporal distributions of H_2O_2 and o-PD concentrations at periodic positions in the central region of the acoustically trapped array. 2D distributions of the H_2O_2 and o-PD concentrations in the viewing region of the acoustic trapping chamber were initially simulated without considering HRP-mediated substrate consumption during the diffusion process. The H_2O_2 concentration in the central observation window positioned ca. 10 mm from the point of substrate injection was calculated as ca. 20 μM after 0.5 h compared with 1 mM for an array containing preloaded H_2O_2. Moreover, although a circular diffusion front was generated initially at the point of injection, the simulations confirmed that a planar chemical front advanced across the microdroplet array (Figures 4B and Figure S7). Significantly, the simulations showed an induction time along the direction of the reaction-diffusion field (x axis) (Figure 4C and Figure S7), consistent with the experimental results displayed in Figure 2E−F. In contrast, minimal differences in the H_2O_2 and o-PD concentrations were observed along the direction perpendicular to the direction of diffusion (Figure 4D,E and Figure S8), in agreement with the data shown in Figure 2G. We used a finite explicit approach involving an iterative procedure to consider the mass transfer balance between the rates of diffusion and HRP-mediated consumption of H_2O_2 and o-PD at each consecutive lattice point. Conversion of the substrates to produce 2,3-DAP

was modeled using the established reaction mechanism (Figures S9−10).[41,42] By simulating the interplay between the peroxidase reaction occurring between neighboring microdroplets and the advancing substrate concentration gradient, we determined the dependency of Δt_{act} on changes in the initial H_2O_2/o-PD molar ratio (Figure S11) or values of the H_2O_2 diffusion coefficient (Figure S12). The simulations showed that Δt_{act} increased nonlinearly with increasing H_2O_2/o-PD molar ratio. This was consistent with experimental data (Figures 2I and 3A,B), and indicated that relatively low levels of o-PD were required to establish an effective reaction-diffusion gradient across the protocell community.

To elicit a spatiotemporal biochemical response via the onset of molecule-based signaling within the droplet arrays, we prepared acoustically patterned PDDA/ATP droplet 2D arrays comprising two spatially separated protocell populations. Two square grid networks of microdroplets comprising either sequestered fluorescein-isothiocyanate (FITC)-tagged GOx (green; population **1**) or RITC-HRP (red; population **2**) were acoustically patterned in different regions of the observation window, and a mixture of glucose and o-PD codiffused into the device from a region near to population **1** (Figure 5A). Interactions between the two separated protocell populations and the substrate concentration gradients established within the viewing region were examined by analyzing the spatiotemporal response associated with the onset of the GOx/HRP tandem reaction, in which glucose and o-PD provided chemical inputs into populations **1** and **2**, respectively, and H_2O_2 acted as an internally generated signaling molecule between the two protocell communities (Figure 5B). Unidirectional codiffusion of the substrates (glucose/o-PD) into population **1** produced a distinct spatiotemporal response in population **2** (Figure 5C). This was consistent with the in situ generation and propagation of a H_2O_2 reaction-diffusion front from the GOx-containing droplets to the spatially separated HRP-containing array to produce a time- and space-dependent response in the production of 2,3-DAP specifically within population **2**. Values of Δt_{act} between adjacent droplets were typically 6 s for the codiffusion system compared with 17 s for the same spatially separated binary population subjected to unidirectional diffusion of o-PD alone into the observation window when preloaded with glucose (Figure 5D). Moreover, we observed different responses in terms of the initial rates of 2,3-DAP production; while the rates were constant for droplets aligned in rows along the direction of codiffusion of glucose/o-PD, the reaction rates decreased when o-PD alone was diffused into the viewing region after preloading with glucose (Figure S13). We attributed this to an increase in the H_2O_2/o-PD molar ratio (Figure 2I) associated with preloading of glucose and the almost instantaneous generation of H_2O_2 in population **1** in the absence of an advancing glucose gradient. In contrast, protocells in population **2** were simultaneously activated when glucose was diffused into population **1** after preloading both populations with a homogeneous concentration of o-PD (Figure 5E) or in the absence of a H_2O_2 and o-PD diffusion gradient (Figure 5F).

DISCUSSION

Acoustically patterned periodic arrays of uniform enzyme-containing coacervate-based protocells exhibit a spatiotemporal biochemical response when exposed to an advancing unidirectional flux of diffusing substrate molecules under non-equilibrium conditions. In essence, the protocell community is able to translate the encoded information in the o-PD and H_2O_2 reaction-diffusion gradient profiles (direction of the diffusion front, initial substrate molar ratios, differences in diffusion coefficients) into specific signal outputs based on different activation and lag times, and nonlinear or linear responses in fluorescence intensity. The sensing behavior can be extended to binary populations of enzyme-containing coacervate microdroplets that are spatially separated within the array but chemically coupled via an internally produced signaling molecule (H_2O_2) that connects the two communities via a concerted biochemical cascade reaction. It should be possible to advance this strategy to more complex arrays by increasing the diversity of distinct protocell populations or integrating more functionalities into each population with the long-term objective of generating synthetic protocell consortia with nonequilibrium cell-like communication networks.[43,44] To this end, the incorporation of microfluidic technologies into the acoustic trapping device to precisely control the concentration gradients across the sample chamber could be highly significant.

Overall, our studies provide a path toward establishing a systematic approach to studying the spatial and temporal interactions of organized communities of synthetic protocells in the presence of propagating reaction-diffusion gradients, and offer a new methodology for exploring the complexity of protocellular communication networks operating under non-equilibrium conditions. More generally, the spatiotemporal response of acoustically trapped microdroplet arrays to coded reaction-diffusion gradients could provide new opportunities for developing organized platforms for chemical and biochemical screening, enzymatic kinetic assays, and clinical diagnostics.

METHODS

Preparation of Enzyme-Containing Coacervate Microdroplet Arrays. One microliter of a premixed solution of PDDA (25 mM monomer) and HRP (0.2 mg mL^{-1}) was gently added to the center of the acoustic trapping chamber containing aqueous ATP (1 mL, 2.5 mM) in the presence of two orthogonal acoustic standing waves (6.76/6.78 MHz, 10 V). After continuous coalescence of primary coacervate droplets over 30 min, a periodic 2D array (ca. 20 × 20) of HRP-containing PDDA/ATP microdroplets was formed specifically at the nodal regions within a localized area close to the point of injection of the PDDA/HRP mixture. Similar procedures were used to prepare two different regions of enzyme-containing coacervate microdroplet arrays within the same observation window. The multicomponent array was prepared in sequence. An organized population of HRP-containing PDDA/ATP droplets was prepared as above, and then an aqueous mixture (4 μL) of PDDA (25 mM monomer) and GOx (0.2 mg mL^{-1}) was injected under the same acoustic standing wave field but at a different location in the ATP-filled chamber so that two spatially separated periodic arrays of PDDA/ATP droplets containing either GOx or HRP could be viewed in the central observation window. Fluorescent enzyme-containing PDDA/ATP coacervate microdroplets were prepared by using RITC-tagged HRP and FITC tagged-GOx.

Coacervate Droplet Array-Based Enzyme Reactions in Chemical Field Gradients. A 2D periodic array of HRP-containing PDDA/ATP coacervate microdroplets was pre-

pared as described above. The supernatant was carefully removed and exchanged with Milli-Q water three times under the same acoustic pressure field. The acoustic field was then switched off, and the enzyme substrates were diffused into the sample chamber (total volume = 1 mL) containing the microdroplet array specifically from one side of the device (the left side as viewed in the Figures). Microscopy images were recorded in the central observation window positioned ca. 10 mm from the point of substrate injection. Several droplet array-based enzyme reaction experiments were undertaken for the single population of HRP-containing microdroplets: (i) codiffusion of H_2O_2 (10 μL; 25, 50, 100, or 200 mM; corresponding final equilibrated concentrations in the acoustic trapping chamber: 0.25, 0.5, 1, and 2 mM) and o-PD (10 μL; 50 mM; final concentration, 0.5 mM) into a 2D array; (ii) single-component diffusion of H_2O_2 (10 μL; 100 mM; final concentration, 1 mM) or o-PD (10 μL; 50 mM; final concentration, 0.5 mM) into a HRP-containing droplet array premixed with a solution of o-PD (10 μL; 50 mM; final concentration, 0.5 mM) or H_2O_2 (10 μL; 100 mM; final concentration, 1 mM), respectively; and (iii) reactions involving no imposed concentration gradients by homogeneous mixing of o-PD (10 μL; 50 mM; final concentration, 0.5 mM) and H_2O_2 (10 μL; 100 mM; final concentration, 1 mM) with a final dilution factor of ×50 in the presence of a microdroplet array. Similarly, enzyme reaction experiments were performed for two spatially separated 2D arrays of HRP- or GOx-containing microdroplets: (i) codiffusion of glucose (10 μL; 100 mM; final concentration, 1 mM) and o-PD (10 μL; 50 mM; final concentration, 0.5 mM) into two spatially separated 2D arrays; (ii) single-component diffusion of glucose (10 μL; 100 mM; final concentration, 1 mM) or o-PD (10 μL; 50 mM; final concentration, 0.5 mM) into two spatially separated arrays premixed with o-PD (10 μL; 50 mM; final concentration, 0.5 mM) or glucose (10 μL; 100 mM; final concentration, 1 mM); and (iii) reactions involving no imposed concentration gradients by homogeneous mixing of o-PD (10 μL; 50 mM; final concentration, 0.5 mM) and glucose (10 μL; 100 mM; final concentration, 1 mM) with a final dilution factor of ×50 in the presence of two spatially separated microdroplet arrays.

■ ASSOCIATED CONTENT

⑤ Supporting Information

The Supporting Information is available free of charge on the [ACS Publications website](#) at DOI: [10.1021/acscentsci.8b00555](#).

> Additional experimental details, methods, and figures including schematic representation, confocal microscopy images, simulation results, reaction mechanism, and analysis of the coacervate droplet array-based enzyme reactions in chemical field gradients ([PDF](#))

■ AUTHOR INFORMATION

Corresponding Author

*E-mail: s.mann@bristol.ac.uk.

ORCID ⊙

Liangfei Tian: 0000-0003-4340-2598

Stephen Mann: 0000-0003-3012-8964

Notes

The authors declare no competing financial interest.

■ REFERENCES

(1) Kholodenko, B. N. Cell-signalling dynamics in time and space. *Nat. Rev. Mol. Cell Biol.* **2006**, 7 (3), 165−176.

(2) Purvis, J. E.; Lahav, G. Encoding and decoding cellular information through signaling dynamics. *Cell* **2013**, 152 (5), 945−956.

(3) Christian, J. L. Morphogen gradients in development: from form to function. *Wiley Interdiscip. Rev. Dev. Biol.* **2012**, 1 (1), 3−15.

(4) Adler, J.; Tso, W. W. "Decision"-making in bacteria: chemotactic response of Escherichia coli to conflicting stimuli. *Science* **1974**, 184 (4143), 1292−4.

(5) Bramkamp, M.; van Baarle, S. Division site selection in rod-shaped bacteria. *Curr. Opin. Microbiol.* **2009**, 12 (6), 683−688.

(6) Semenov, S. N.; Markvoort, A. J.; de Greef, T. F. A.; Huck, W. T. S. Threshold sensing through a synthetic enzymatic reaction−diffusion network. *Angew. Chem., Int. Ed.* **2014**, 53 (31), 8066−8069.

(7) Karzbrun, E.; Tayar, A. M.; Noireaux, V.; Bar-Ziv, R. H. Programmable on-chip DNA compartments as artificial cells. *Science* **2014**, 345 (6198), 829−832.

(8) Litschel, T.; Norton, M. M.; Tserunyan, V.; Fraden, S. Engineering reaction−diffusion networks with properties of neural tissue. *Lab Chip* **2018**, 18 (5), 714−722.

(9) Weitz, M.; Mückl, A.; Kapsner, K.; Berg, R.; Meyer, A.; Simmel, F. C. Communication and computation by bacteria compartmentalized within microemulsion droplets. *J. Am. Chem. Soc.* **2014**, 136 (1), 72−75.

(10) Li, M.; Huang, X.; Tang, T.-Y. D.; Mann, S. Synthetic cellularity based on non-lipid micro-compartments and protocell models. *Curr. Opin. Chem. Biol.* **2014**, 22, 1−11.

(11) Tu, Y.; Peng, F.; Adawy, A.; Men, Y.; Abdelmohsen, L. K.; Wilson, D. A. Mimicking the cell: bio-inspired functions of supramolecular assemblies. *Chem. Rev.* **2016**, 116 (4), 2023−2078.

(12) Szostak, J. W. The narrow road to the deep past: in search of the chemistry of the origin of life. *Angew. Chem., Int. Ed.* **2017**, 56 (37), 11037−11043.

(13) Buddingh, B. C.; van Hest, J. C. M. Artificial cells: synthetic compartments with life-like functionality and adaptivity. *Acc. Chem. Res.* **2017**, 50 (4), 769−777.

(14) Schwille, P. How simple could life be? *Angew. Chem., Int. Ed.* **2017**, 56 (37), 10998−11002.

(15) Mann, S. Life as a nanoscale phenomenon. *Angew. Chem., Int. Ed.* **2008**, 47 (29), 5306−5320.

(16) Grzybowski, B. A.; Huck, W. T. S. The nanotechnology of life-inspired systems. *Nat. Nanotechnol.* **2016**, 11 (7), 585−592.

(17) Merindol, R.; Walther, A. Materials learning from life: concepts for active, adaptive and autonomous molecular systems. *Chem. Soc. Rev.* **2017**, 46 (18), 5588−5619.

(18) Lubbe, A. S.; van Leeuwen, T.; Wezenberg, S. J.; Feringa, B. Designing dynamic functional molecular systems. *Tetrahedron* **2017**, 73 (33), 4837−4848.

(19) Li, M.; Harbron, R. L.; Weaver, J. V.; Binks, B. P.; Mann, S. Electrostatically gated membrane permeability in inorganic protocells. *Nat. Chem.* **2013**, 5 (6), 529−536.

(20) Li, M.; Huang, X.; Mann, S. Spontaneous growth and division in self-reproducing inorganic colloidosomes. *Small* **2014**, 10 (16), 3291−3298.

(21) Peters, R. J. R. W.; Nijemeisland, M.; van Hest, J. C. M. Reversibly Triggered Protein-Ligand Assemblies in Giant Vesicles. *Angew. Chem., Int. Ed.* **2015**, *54* (33), 9614−9617.

(22) Tamate, R.; Ueki, T.; Yoshida, R. Evolved colloidosomes undergoing cell-like autonomous shape oscillations with buckling. *Angew. Chem., Int. Ed.* **2016**, *55* (17), 5179−5183.

(23) Wang, S.; Li, M.; Patil, A. J.; Sun, S.; Tian, L.; Zhang, D.; Cao, M.; Mann, S. Design and construction of artificial photoresponsive protocells capable of converting day light to chemical energy. *J. Mater. Chem. A* **2017**, *5* (47), 24612−24616.

(24) Sun, S.; Li, M.; Dong, F.; Wang, S.; Tian, L.; Mann, S. Chemical signaling and functional activation in colloidosome-based protocells. *Small* **2016**, *12* (14), 1920−1927.

(25) Qiao, Y.; Li, M.; Booth, R.; Mann, S. Predatory behaviour in synthetic protocell communities. *Nat. Chem.* **2017**, *9* (2), 110−119.

(26) Rodriguez-Arco, L.; Li, M.; Mann, S. Phagocytosis-inspired behaviour in synthetic protocell communities of compartmentalized colloidal objects. *Nat. Mater.* **2017**, *16* (8), 857−863.

(27) Adamala, K. P.; Martin-Alarcon, D. A.; Guthrie-Honea, K. R.; Boyden, E. S. Engineering genetic circuit interactions within and between synthetic minimal cells. *Nat. Chem.* **2016**, *9* (5), 431−439.

(28) Gardner, P. M.; Winzer, K.; Davis, B. G. Sugar synthesis in a protocellular model leads to a cell signalling response in bacteria. *Nat. Chem.* **2009**, *1* (5), 377−383.

(29) Lentini, R.; Santero, S. P.; Chizzolini, F.; Cecchi, D.; Fontana, J.; Marchioretto, M.; Del Bianco, C.; Terrell, J. L.; Spencer, A. C.; Martini, L.; Forlin, M.; Assfalg, M.; Dalla Serra, M.; Bentley, W. E.; Mansy, S. S. Integrating artificial with natural cells to translate chemical messages that direct E-coli behaviour. *Nat. Commun.* **2014**, *5*, 4012.

(30) Koga, S.; Williams, D. S.; Perriman, A. W.; Mann, S. Peptide-nucleotide microdroplets as a step towards a membrane-free protocell model. *Nat. Chem.* **2011**, *3* (9), 720−724.

(31) Tang, T.-Y. D.; Rohaida Che Hak, C.; Thompson, A. J.; Kuimova, M. K.; Williams, D. S.; Perriman, A. W.; Mann, S. Fatty acid membrane assembly on coacervate microdroplets as a step towards a hybrid protocell model. *Nat. Chem.* **2014**, *6* (6), 527−533.

(32) Aumiller, W. M.; Keating, C. D. Phosphorylation-mediated RNA/peptide complex coacervation as a model for intracellular liquid organelles. *Nat. Chem.* **2016**, *8* (2), 129−137.

(33) Mason, A. F.; Buddingh, B. C.; Williams, D. S.; van Hest, J. C. M. Hierarchical self-assembly of a copolymer-stabilized coacervate protocell. *J. Am. Chem. Soc.* **2017**, *139* (48), 17309−17312.

(34) Nakashima, K. K.; Baaij, J. F.; Spruijt, E. Reversible generation of coacervate droplets in an enzymatic network. *Soft Matter* **2018**, *14* (3), 361−367.

(35) Crosby, J.; Treadwell, T.; Hammerton, M.; Vasilakis, K.; Crump, M. P.; Williams, D. S.; Mann, S. Stabilization and enhanced reactivity of actinorhodin polyketide synthase minimal complex in polymer-nucleotide coacervate droplets. *Chem. Commun.* **2012**, *48* (97), 11832−11834.

(36) Tang, T.-Y. D.; van Swaay, D.; deMello, A.; Ross Anderson, J. L.; Mann, S. In vitro gene expression within membrane-free coacervate protocells. *Chem. Commun.* **2015**, *51* (57), 11429−11432.

(37) Yin, Y.; Niu, L.; Zhu, X.; Zhao, M.; Zhang, Z.; Mann, S.; Liang, D. Non-equilibrium behaviour in coacervate-based protocells under electric-field-induced excitation. *Nat. Commun.* **2016**, *7*, 10658.

(38) Tian, L.; Martin, N.; Bassindale, P. G.; Patil, A. J.; Li, M.; Barnes, A.; Drinkwater, B. W.; Mann, S. Spontaneous assembly of chemically encoded two-dimensional coacervate droplet arrays by acoustic wave patterning. *Nat. Commun.* **2016**, *7*, 13068.

(39) Kuchler, A.; Yoshimoto, M.; Luginbuhl, S.; Mavelli, F.; Walde, P. Enzymatic reactions in confined environments. *Nat. Nanotechnol.* **2016**, *11* (5), 409−420.

(40) Williams, D. S.; Patil, A. J.; Mann, S. Spontaneous structuration in coacervate-based protocells by polyoxometalate-mediated membrane assembly. *Small* **2014**, *10* (9), 1830.

(41) Rodriguez-Lopez, J. N.; Gilabert, M. A.; Tudela, J.; Thorneley, R. N. F.; Garcia-Canovas, F. Reactivity of horseradish peroxidase compound II toward substrates: kinetic evidence for a two-step mechanism. *Biochemistry* **2000**, *39* (43), 13201−13209.

(42) Liu, H.; Wang, Z.; Liu, Y.; Xiao, J.; Wang, C. Enthalpy change and mechanism of oxidation of o-phenylenediamine by hydrogen peroxide catalyzed by horseradish peroxidase. *Thermochim. Acta* **2006**, *443* (2), 173−178.

(43) Shum, H.; Yashin, V. V.; Balazs, A. C. Self-assembly of microcapsules regulated via the repressilator signaling network. *Soft Matter* **2015**, *11* (18), 3542−3549.

(44) Kolmakov, G. V.; Yashin, V. V.; Levitan, S. P.; Balazs, A. C. Designing communicating colonies of biomimetic microcapsules. *Proc. Natl. Acad. Sci. U. S. A.* **2010**, *107* (28), 12417−12422.